

Modelling the size and strength benefits of optimised step/scarf joints and repairs in composite structures

Robert S. Pierce^{a,b,c*} and Brian G. Falzon^{a,b}

^a Northern Ireland Advanced Composites and Engineering (NIACE) centre, 5 Airport Road, Belfast, United Kingdom, BT3 9EF

^b Advanced Composites Research Group, School of Mechanical and Aerospace Engineering, Queen's University Belfast, United Kingdom, BT9 5AH

^c Department of Mechanical, Materials and Manufacturing Engineering, University of Nottingham Ningbo China, University Park, Ningbo, P.R. China, 315100.

* Corresponding author. Address: Department of Mechanical, Materials and Manufacturing Engineering, University of Nottingham Ningbo China, University Park, Ningbo, P.R. China, 315100.

Email: Robert.pierce@nottingham.edu.cn

Phone: +86 574 8818 0000 (ex. 8834)

Abstract

Adhesive bonding offers a better load transfer between adherends, for the assembly and repair of composite structures, compared with mechanical fastening methods. One drawback of adhesive bonded repairs is the considerable amount of material which must be removed, around the damaged region, to ensure adequate load transfer. Optimised geometries that account for the highly-orthotropic properties of individual composite plies are investigated, including a novel 'fibre-oriented' *scarf* approach that is inspired by an existing fibre-oriented *step* design. These methods aim to reduce the length of joint and repair bonding regions by at least 36%, compared with conventional step and scarf geometries of a similar strength.

Size-reduction benefits are predicted using a MATLAB tool that is applicable for any composite laminate, and parametric analysis used to assess the effect of ply thickness, the number of plies, stacking sequence and taper angle.

Cohesive Zone Models of joints and repairs with conventional and fibre-oriented designs are used to predict and compare the ultimate strength of each configuration. The existing fibre-oriented step design appears to show no benefit over a conventional step design. However, the novel fibre-oriented scarf approach results in a 33-40% reduction in the size of the bonding region compared to a conventional scarf design with similar strength. Analysis further indicates a 17-22% increase in ultimate strength for joints and repairs with the same bonding region size that employ the optimised fibre-oriented scarf design.

Keywords: B. Adhesion, E. Joints/joining, C. Finite element analysis (FEA), Scarf repair.

1 Introduction

In the assembly and repair of composite structures, adhesive bonding methods offer significant advantages over mechanical fastening methods, particularly for large-scale aerospace applications [1]. Common tapered step/scarf methods offer improved loading efficiency, reduced drilling and a minimal change to the surface profile of a structure [2]. However, these methods often require significant material removal and rely on operator expertise. This has motivated considerable research into the design, optimisation and verification of adhesively bonded joints and repairs via numerical modelling.

1.1 *Modelling of joints and repairs*

The modelling of adhesively bonded joints and repairs in composite structures is complicated by material behaviour that occurs over a range of different scales. Firstly, composite plies have highly orthotropic mechanical behaviour that needs to be modelled accurately, however each ply is very thin relative to the typical size of a complete structure. Secondly, a shallow taper angle is required for efficient load transfer across an adhesive bonding interface, but this can result in an interface over 300 times longer than it is thick. For example, a 3° scarf repair (an industry standard) in a relatively thin laminate of 16 plies (each 0.15 mm thick), with a 0.15 mm thick adhesive, requires a 45 mm long bonding region. Also, the variability of adhesive thickness, scarf tip geometry and step corner shape that are seen in real repairs [3], all need to be idealised for the purposes of numerical modelling.

The need to model individual ply and adhesive behaviour with shallow taper angles therefore makes 3D modelling of realistic step/scarf repairs difficult, as a very large number of elements are usually required.

A common simplification for comparative studies and preliminary design, is to model and test a two-dimensional cross-section of the repair interface through the principal loading direction [1]. This forms what is often called a 2D 'representative joint', and can greatly reduce the complexity and computational effort required for full 3D repair modelling. Subsequently, adhesively bonded joints and repairs are often studied together, since the former represents a simplification of the latter.

It is important to note however, that 2D representative joints tend to be overly conservative, as they neglect any 3D load re-distribution that occurs during plastic adhesive deformation [4]. Research has shown that the ultimate strength of a representative joint can be up to 40% less than that of a similar 3D repair as a result of increased shear stresses in the adhesive interface [5]. Hence, both representative joints and full 3D repair cases should be considered for the optimisation of adhesively bonded repairs.

1.2 Repair design optimisation

The optimisation of the shape, size and stacking sequence for adhesively bonded step/scarf repairs has received considerable attention from the research community in recent years [6–11]. Conventionally, bonded step/scarf repairs rely on the cutting of a circular shape with a constant taper, in the parent material containing the damage, and the introduction of a patch with a stacking sequence that matches that of the parent laminate. In high performance structures, a taper angle of 1.91° or 2.86° (equivalent to a taper ratio of 30:1 or 20:1) is common, although even shallower taper angles of 1.145° (50:1) may be used [6,7]. Reducing taper angle theoretically increases the efficiency of load transfer and overall bond strength, however it also requires a greater volume of material removal and subsequently reduces the residual strength of the parent laminate. Over-ply are also commonly employed to strengthen step/scarf repairs, as they provide an additional load path and help seal and protect the thin edges of the repair patch. The use of one over-ply for every 16 plies in the parent laminate has been recommended [8], where the first over-ply should match the orientation of the outermost parent ply [9].

Previous studies have also evaluated repairs where the patch stacking sequence varies from that of the parent laminate. In one case, highly customised stacking sequences in the repair patch were shown to improve tensile strength by 30% compared to a ply-matched 2.85° scarf repair, for an overall repair efficiency of 85% [9]. Other work involving a parametric study of stacking sequence, laminate thickness, ply matching, adhesive thickness and over-ply for 5° scarf repairs found that there was a relatively low sensitivity to mismatched plies across the bonding interface [10]. This research also supported the use of over-ply for the reduction of peak stresses in the adhesive.

With regards to the shape of adhesively bonded step/scarf repairs, Wang and Gunnion [11] have investigated elliptical and mixed square-ellipse designs with variable taper angles. Such geometries can significantly reduce the repair size and material removal requirements for structures with orthotropic loading, where a traditional circular patch is overly conservative.

More recently, the development of automated mobile 3- and 5-axis milling machines has allowed for greater complexity in the design of adhesively bonded repairs [12]. In particular, researchers have proposed a 'fibre-oriented' step design, where steps are machined only in the fibre direction of each ply, since the strength contribution of steps transverse to the fibre direction is considered to be negligible [12,13]. This results in reduced material removal and a repair area up to 50% smaller than a conventional step design, with theoretically equivalent strength. Initial mechanical test results, for representative joints, have shown that the tensile strength of fibre-oriented step joints can match that of traditional step joints that are 40% longer, both with and without over-ply [14]. However, even with a very shallow taper (50:1 or 1.145°), these joints were only capable of restoring 59% and 54% of the pristine tensile strength of the parent laminate with and without over-ply, respectively.

This paper investigates the potential of the fibre-oriented step approach for both joints and 3D repairs using numerical modelling techniques. This concept is extended to the development of a novel fibre-oriented scarf design that aims to provide greater overall repair efficiency.

2 Fibre-oriented machining for joints and repairs

2.1 Fibre-oriented step design

Recent work by Niedernhuber et al. [14] proposed that composite step repairs may be optimised by employing a fibre-oriented step approach, where step lengths for each ply are shortened based on the orientation of fibres in each ply relative to the bonding direction, as shown in

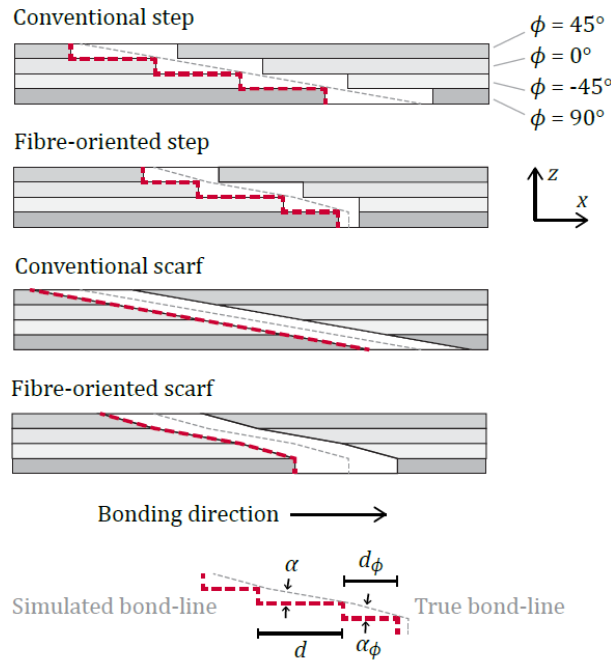


Figure 1. This relationship is summarised in Equation (1), which defines the appropriate step length for any fibre-oriented ply, d_ϕ , based on the fibre direction in that ply, ϕ , the ply thickness, t_p , and the ideal minimum taper angle, α , that would be used for a conventional step approach. In this paper, the term “bonding direction” is used to represent the direction of the transition between parent and patch

material, within the plane of the laminate, as shown in

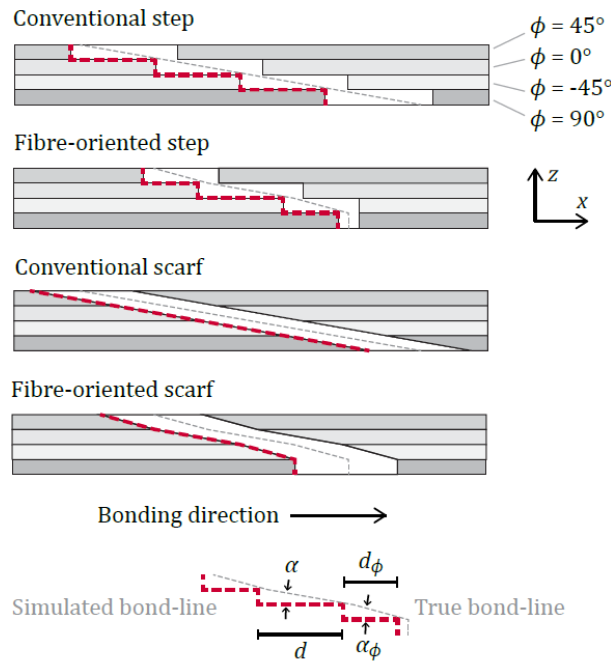


Figure 1. For a quasi-2D joint the bonding direction is consistent across the width of the joint, but for a circular 3D repair the bonding direction changes radially, always pointing towards the centre of the repair patch within the plane of the laminate.

$$d_{\phi} = t_p \frac{\cos \phi}{\tan \alpha} \quad (1)$$

Hence, for a 0° ply aligned with the bonding direction, the fibre-oriented step length will be equivalent to that of a conventional step. However, as the alignment of individual plies deviates from the bonding direction, this step length reduces. Thus, plies $\pm 45^{\circ}$ relative to the bonding direction will have a 29.3% shorter step length, and plies 90° to the bonding direction will have no step length at all (resulting in a 2-ply drop).

Theoretically, since the fibres carry the bulk of the loading in these structures, it is essential to maintain the length of the adhesive interface along the fibre direction. However areas of reduced stress, such as those where the bonding direction is perpendicular to the fibre direction, can have shorter steps in order to reduce the overall size of the repair. This size reduction is the dominant motivation for a fibre-oriented step design that achieves a theoretically similar strength.

2.2 Fibre-oriented scarf design

In this work, the benefits of a fibre-oriented *step* design are extended to a fibre-oriented *scarf* design, where the scarf angle of each ply, α_ϕ , varies relative to the bonding direction, according to Equation (2), the fibre direction in that ply, ϕ , and the ideal minimum taper angle, α .

$$\alpha_\phi = \tan^{-1} \left(\frac{\tan \alpha}{\cos \phi} \right) \quad (2)$$

Hence, the scarf angle in each ply is seen to increase from the ideal minimum, α , as the fibre direction deviates from the bonding direction. At an extreme, when this deviation is orthogonal (at 90°), the fibre-oriented scarf angle of the ply also becomes 90° , appearing as a step rather than a scarf.

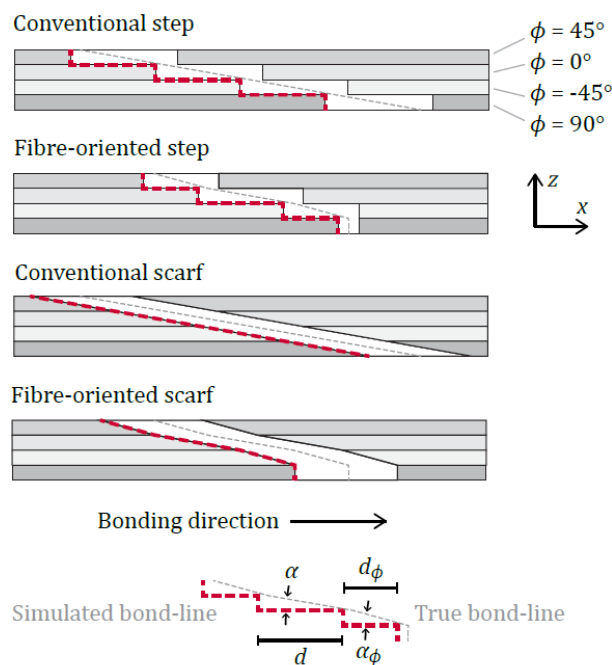


Figure 1 demonstrates the cross-sections of the four different bonding configurations (conventional step, conventional scarf, fibre-oriented step and fibre-oriented scarf) for similar $[45^\circ, 0^\circ, -45^\circ, 90^\circ]$ laminates with the same minimum taper angle, α .

The fibre-oriented scarf configuration aims to further optimise the design of bonded repairs by combining the greater efficiency of a scarf approach with the reduced size of a fibre-oriented step approach. This research investigates the benefits of fibre-oriented step/scarf methods compared with

conventional step/scarf repairs, in terms of both size and strength, via parametric and Cohesive Zone Modelling respectively.

3 Predictive tool for the design of fibre-oriented repairs

A MATLAB code has been developed in order to predict the fibre-oriented step/scarf profiles for each ply in a given laminate. This requires knowledge of the stacking sequence, ply thickness, damage area and desired minimum taper angle. Each ply profile is identical for both fibre-oriented designs, only the through-thickness ply transitions between ply profiles are different. Figure 2 demonstrates the ply profiles for a fibre-oriented repair in a $[45^\circ, 0^\circ, -45^\circ, 90^\circ]_{2s}$ laminate, compared against a conventional step/scarf repair design. Due to the simplicity and speed of this code, it has also been used to conduct a parametric analysis on the sensitivity of overall repair size to each input parameter.

3.1 MATLAB code

With reference to Figure 3, the MATLAB code first requires the definition of an initial damage envelope in polar coordinates (p_0, θ) . For this research a constant circular envelope has been assumed, however the code will work just as well for any elliptical shape that would be common for a scarf repair. Each successive ply profile, p_i , is defined using a finite number of polar coordinates. In order to minimise any discretisation error, a resolution of 0.001° is used between the j^{th} and $j + 1^{\text{th}}$ coordinates of all ply profiles, as shown in Figure 3. Hence, each ply profile is defined by a series of around 360,000 points, each spaced 0.001° apart.

Based on user input for the desired minimum taper angle, α , and ply thickness, t_p , the step/scarf length in the fibre direction, d , can be calculated according to Equation (3), and is shown in Figure 4.

$$d = \frac{t_p}{\tan \alpha} \quad (3)$$

The profile for each ply, p_i , can be determined sequentially, based on its fibre orientation, ϕ_i , and the profile of the previous ply, p_{i-1} . Effectively this process can be divided into 5 steps, as depicted in Figure 4.

Firstly, two intercept points (red dots in Figure 4) need to be identified. These occur where the tangent line of the previous ply profile, p_{i-1} , is parallel to the fibre orientation of the current ply, ϕ_i , as shown in

the first step of Figure 4. The intercept points are located by calculating the x-y gradient at all points, j , of the previous ply profile in Cartesian coordinates, using a central difference scheme, Equation (4), which are then compared with the tangent of the fibre orientation. The two intercept points are labelled “high” and “low” based on their relative location in polar space, and defined by radii, p_i^{intH} and p_i^{intL} respectively, at corresponding angles, θ_i^{intH} and θ_i^{intL} , in Equations (5) and (6).

$$\left. \frac{dy}{dx} \right|_{i-1}^j = \frac{p^{j+1} \sin \theta^{j+1} - p^{j-1} \sin \theta^{j-1}}{p^{j+1} \cos \theta^{j+1} - p^{j-1} \cos \theta^{j-1}} \Bigg|_{i-1}^j \quad (4)$$

$$p_i^{intH} = p_{i-1}^j, \quad \theta_i^{intH} = \theta_{i-1}^j, \quad \text{where } \left. \frac{dy}{dx} \right|_{i-1}^j = \tan \phi_i, \quad \text{for } 0^\circ < \theta_{i-1}^j \leq 180^\circ \quad (5)$$

$$p_i^{intL} = p_{i-1}^j, \quad \theta_i^{intL} = \theta_{i-1}^j, \quad \text{where } \left. \frac{dy}{dx} \right|_{i-1}^j = \tan \phi_i, \quad \text{for } -180^\circ < \theta_{i-1}^j \leq 0^\circ \quad (6)$$

The profile of the current ply, p_i , can be defined by two straight segments and two arc/irregular segments. The straight segments remain parallel to the current ply orientation with their midpoints at the intercept points. The arc/irregular segments match the profile of the previous ply between intercept points, but are shifted by the step/scarf length in the ply orientation direction. Therefore, the angular locations of four nodes need to be defined in polar coordinates for the joints between these straight and curved segments, according to Equations (7), (8), (9) and (10). This represents the second step in Figure 4.

$$\theta_i^{joint 1} = \tan^{-1} \left(\frac{p_i^{intL} \sin \theta_i^{intL} + d \sin \phi_i}{p_i^{intL} \cos \theta_i^{intL} - d \cos \phi_i} \right) \quad (7)$$

$$\theta_i^{joint 2} = \tan^{-1} \left(\frac{p_i^{intH} \sin \theta_i^{intH} + d \sin \phi_i}{p_i^{intH} \cos \theta_i^{intH} - d \cos \phi_i} \right) \quad (8)$$

$$\theta_i^{joint 3} = \tan^{-1} \left(\frac{p_i^{intH} \sin \theta_i^{intH} - d \sin \phi_i}{p_i^{intH} \cos \theta_i^{intH} + d \cos \phi_i} \right) \quad (9)$$

$$\theta_i^{joint 4} = \tan^{-1} \left(\frac{p_i^{intL} \sin \theta_i^{intL} - d \sin \phi_i}{p_i^{intL} \cos \theta_i^{intL} + d \cos \phi_i} \right) \quad (10)$$

Once these angular locations of the joint nodes are known, the two straight segments, $p_i^{str 1}$ and $p_i^{str 2}$, that remain parallel to the fibre direction of the current ply can be defined by Equations (11) and (12), as shown in step 3 of Figure 4.

$$p_i^{str 1} = -q_i \frac{\cos \phi_i}{\sin(\theta_i - \phi_i)}, \quad \text{for } \theta_i^{joint 4} < \theta_i \leq \theta_i^{joint 1} \quad (11)$$

$$p_i^{str 2} = q_i \frac{\cos \phi_i}{\sin(\theta_i - \phi_i)}, \quad \text{for } \theta_i^{joint 2} < \theta_i \leq \theta_i^{joint 3} \quad (12)$$

where,

$$q_i = p_i^{intL} |\sin \theta_i^{intL}| + p_i^{intL} |\cos \theta_i^{intL}| \times |\tan \phi_i| \quad (13)$$

Next the two arc/irregular segments, $p_i^{arc 1}$ and $p_i^{arc 2}$, can be defined based on the polar profile of the previous ply, p_{i-1} and θ_{i-1} , and the fibre direction of the current ply, ϕ_i , according to Equations (14) and (15). This is reflected by step 4 of Figure 4.

$$p_i^{arc 1} = \sqrt{(p_{i-1} \cos \theta_{i-1} + d \cos \phi_i)^2 + (p_{i-1} \sin \theta_{i-1} + d \sin \phi_i)^2}, \quad (14)$$

$$\text{for } \theta_i^{intL} < \theta_{i-1} \leq \theta_i^{intH}$$

$$p_i^{arc 2} = \sqrt{(p_{i-1} \cos \theta_{i-1} + d \cos \phi_i)^2 + (p_{i-1} \sin \theta_{i-1} + d \sin \phi_i)^2}, \quad (15)$$

$$\text{for } \theta_i^{intH} < \theta_{i-1} \leq \theta_i^{intL}$$

Finally, all four segments can be combined to create the complete radial profile for the current ply in Equation (16), which can be seen in step 5 of Figure 4.

$$p_i = p_i^{arc 1} + p_i^{str 2} + p_i^{arc 2} + p_i^{str 1} \quad (16)$$

This process can then be repeated sequentially for each ply in the full composite layup, where i simply becomes $i + 1$ for the next step. After the final ply profile, p_n , has been determined for a laminate with n plies, the total size of the fibre-oriented scarf repair can be defined by Equation (17) and approximated with a numerical integration method. In this case the trapezoidal rule has been employed.

$$A_{FOsc} = \int_{-\pi}^{\pi} \frac{1}{2} (p_n)^2 d\theta \quad (17)$$

3.2 Parametric analysis of repair size reduction

A parametric study was undertaken in order to assess the size and material removal benefits that result from a fibre-oriented repair design compared with a conventional step/scarf approach. This analysis investigated the effect of ply thickness, taper angle, initial damage envelope size, number of plies and stacking sequence on the scarf area reduction of the repair. In total, around 940 cases were considered based on combinations of the variables outlined in Table 1. The symmetry or asymmetry of a given stacking sequence was also considered, but has no noticeable effect on the size of the fibre-oriented repair. Baseline parameters of a 3° taper, 0.2 mm ply thickness and an 8 ply [45°, 0°, -45°, 90°]_s layup were maintained for the majority of cases.

For each repair configuration the required scarfing area for a fibre-oriented design was compared with that of a conventional scarf, to determine the scarf area reduction, *SAR*, according to Equation (18). Note, this scarf area reduction ignores the initial damage area that is common to both configurations ($\pi(p_0)^2$).

$$SAR = \frac{A_{FOsc} - A_{sc}}{A_{sc} - \pi(p_0)^2} \quad (18)$$

Where the conventional scarf area, A_{sc} , is defined by Equation (19).

$$A_{sc} = \pi(p_0 + nd)^2 \quad (19)$$

Figure 5 shows the scarf area reduction, *SAR*, resulting from changes in minimum taper angle, ply thickness and number of plies, relative to the initial damage radius. Intuitively, increasing ply thickness, number of plies and reducing taper angle all result in a greater scarf area reduction when using a fibre-oriented design compared with a conventional constant taper scarf. These effects are most sensitive to a smaller initial damage radius.

The effect of stacking sequence can be seen in Figure 6, where the quasi-isotropic $[45^\circ, 0^\circ, -45^\circ, 90^\circ]_s$ stacking sequence provides the minimum benefit in scarf area reduction and the unidirectional $[0^\circ]_8$ layup shows the greatest benefit. Hence, it appears that the fibre-oriented step/scarf repair design is even more pertinent for laminates with a large number of plies aligned in one direction. All other stacking sequences appear to fall within this range.

Ultimately, all cases from Table 1 show asymptotic behaviour with increasing damage radius, suggesting that there is an absolute minimum benefit from the fibre-oriented design in terms of scarf area reduction. This asymptote derives from the change of length in each ply step/scarf based on the relative angle between the fibre direction and bonding direction. This change in the step/scarf length is depicted in Figure 7. Where d , defined in Equation (3), represents the step/scarf length in the fibre direction, and d_β represents the step/scarf length in the direction β degrees from the fibre direction.

Subsequently, the relative difference in ply step/scarf length between a fibre-oriented repair and a conventional step/scarf repair can be calculated for any direction, β , according to Equation (20).

$$\frac{d_\beta - d}{d} = \frac{\frac{t_p \cos \beta}{\tan \alpha} - \frac{t_p}{\tan \alpha}}{\frac{t_p}{\tan \alpha}} = \cos \beta - 1 \quad (20)$$

By taking the integral of this relative length change over the range $-\frac{\pi}{2}$ to $\frac{\pi}{2}$, the asymptotic value of the relative area reduction can be calculated with Equation (21). This represents the minimum scarf area reduction that results from using a fibre-oriented step/scarf design, without accounting for the size of the initial damage.

$$\frac{1}{\pi} \int_{-\frac{\pi}{2}}^{\frac{\pi}{2}} \cos \beta - 1 \, d\beta = \frac{2}{\pi} - 1 = -36.34 \% \quad (21)$$

In reality, if the size of the initial damage is very large compared to the overall scarfing area, the benefits of a fibre-oriented step/scarf design may become marginal. This is shown in Figure 8, where the overall repair size reduction resulting from a fibre-oriented design is compared against the minimum taper angle and the ratio of damage radius to composite thickness. This provides a quick and effective tool to

determine the total size benefits of a fibre-oriented repair. For example, a shallow (2°) taper fibre-oriented repair for tool drop damage (with a radius 6-10 times larger than the composite thickness) would be expected to be 25-30% smaller than that of a conventional scarf repair.

4 Cohesive Zone Modelling

4.1 Method

Joint and repair simulations were executed using Abaqus Explicit with a surface-based cohesive interaction between composite adherends. The composite parent and patch components were all modelled with an 8 ply $[45^\circ, 0^\circ, -45^\circ, 90^\circ]_s$ quasi-isotropic layup. The individual plies of each lamina were modelled as separate 0.15 mm thick partitions with properties defined in Table 2, based on values from literature [15].

Models were run using this explicit solver under quasi-static conditions to best account for the non-linearity of the cohesive behaviour model. To enhance computational efficiency, a 0.005 step time was used with semi-automatic mass scaling to ensure a minimum increment time of $1e-8$ from the beginning of the load step. A surface-based cohesive interaction was defined by uncoupled traction-separation behaviour. Damage initiation was based on quadratic traction (maximum nominal stress), and damage evolution was modelled using an energy-based, linear softening behaviour. The material properties for this cohesive behaviour are defined in Table 3, based on values for a brittle Araldite® AV138 adhesive from literature [16]. As a zero-thickness cohesive interaction was used in this model, the K_{nn} , K_{ss} and K_{tt} properties were calculated by dividing the tensile and shear moduli of the adhesive by the 0.2 mm adhesive thickness ($K_{nn} = E/t_a$ and $K_{ss} = K_{tt} = G/t_a$ respectively) as is common for such a Cohesive Zone Model [17].

This modelling approach was validated against recent experimental and numerical results from literature for a lap joint configuration [16], where excellent agreement was observed. Once validated, the same fundamental modelling approach was used for both joint and repair cases.

4.2 Quasi-2D joint modelling

Representative joint models were first developed as they allow for a considerable reduction in geometric and meshing complexity by maintaining a constant cross-section similar to

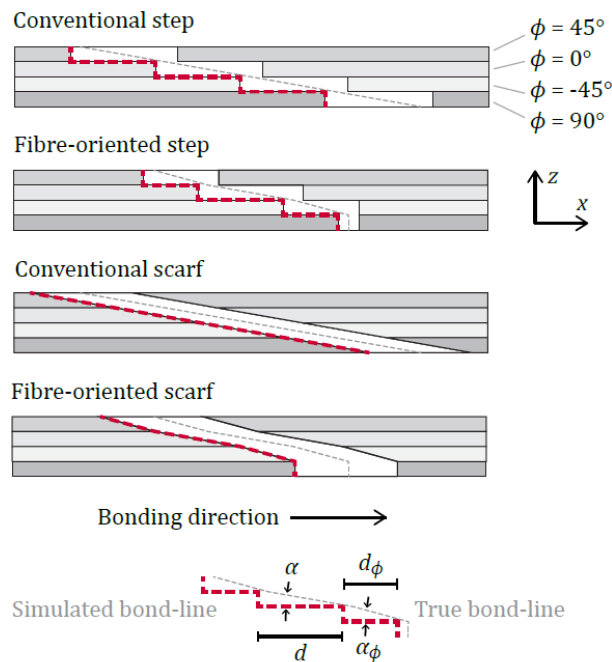


Figure 1, across the width of the joints. Although the problem is essentially 2D, the composite adherends were modelled in 3D to properly define the fibre orientation of each ply, and cohesive surfaces were defined across the faces of the adhesive bonding region. The combined geometry of the simulated coupons was 50 x 10 x 1.2 mm. A 0.5 mm extension was applied gradually to the end of one adherend, in order to induce failure, while the end of the other adherend remained fixed. Meshes were generated with a combination of C3D8R hex and C3D6R wedge elements for a total of around 35,000 elements in each case. This was found to be an optimal mesh density for solution time and accuracy based on mesh convergence analysis.

4.3 3D repair modelling

In the more complex case of the full 3D repair, the total geometry of the parent containing a central repair patch was 140 x 140 x 1.2 mm. Similar to the joint models, a tensile load was applied to one end of the parent laminate while the opposite end remained fixed. Modelling and meshing of the fibre-oriented scarf geometries was particularly challenging. The asymmetry of the fibre-oriented scarf design eliminated the possibility of using symmetric boundary conditions that would normally help reduce computational requirements. Furthermore, the complex and shallow curvature of the ply scarfing also

necessitated advanced partitioning of the scarf region into 8 even 45° arc segments, to allow for swept meshing. Each ply also had to be partitioned several times parallel to the Z-plane in order to enforce the generation of a 4-element-thick mesh per ply. Ultimately, even with considerable mesh optimisation away from the bonding region, a total of 250,000-400,000 elements (C3D8R hex and C3D6R wedge) were necessary to produce reliable results for the full 3D repair models.

5 Quasi-2D joint analysis results

5.1 Ultimate strength

In all joint configurations, the peak stresses were consistently observed either directly between, or adjacent to, the 0° plies that carry the majority of the load. Subsequently, failure of the cohesive interaction was also seen to initiate in the region between 0° plies. The ultimate strength of the four different joint configurations was assessed for a range of taper angles (2°, 3°, 5° and 8°). This relied on the measurement of reaction forces that build up at the ends of the adherends and peak immediately prior to failure. Since the fibre-oriented joint designs had a variable taper in the bonding interfaces, they have been labelled in the results by the minimum taper angle between 0° plies within the joint.

Figure 9 shows the predicted joint strength for each step and fibre-oriented step design at various taper angles, relative to the ply-normalised joint length. Overall, these results suggest that the fibre-oriented step design provides little benefit over conventional step joints, for the full range of taper angles.

Notably however, the difference in strength between step joints with 2° and 3° tapers is relatively small, at less than 10%. This suggests that experimental testing of shallow-taper samples might not reveal a considerable difference between the step and fibre-oriented step designs.

In contrast, modelling predicts the fibre-oriented scarf joints to provide a considerable benefit over the conventional scarf joints, Figure 10,. For example, a fibre-oriented scarf design with a minimum 2° taper is anticipated to yield a 40% reduction in joint length, compared to a similarly strong conventional 2° scarf joint. Another interpretation reveals the same novel design to result in a 22% increase in ultimate strength compared with a regular scarf of the same length. In general, the optimised and conventional scarf designs are both predicted to be 15-35% stronger than their counterpart step designs.

6 3D repair analysis results

6.1 *Ultimate strength*

Similar to the joint analysis results, peak stresses were seen to occur near the highly loaded 0° plies for all repair configurations. Again, the reaction forces were summed across the loaded face of each model in order to calculate the ultimate strength of the repair, immediately prior to failure.

As seen in Figure 11, the fibre-oriented step design is predicted to result in a similar, or even lower, ultimate strength than a conventional step repair of similar length. In contrast, the fibre-oriented scarf modelling results predict a significant benefit over the conventional scarf repairs. Compared with a conventional scarf repair of a similar size or strength, the fibre-oriented scarf with a 2° minimum taper is predicted to be 17% stronger or 33% smaller, respectively. Overall, as expected, the scarf-based methods are seen to perform better than the step-based designs.

6.2 *Failure analysis*

By monitoring the quadratic stress damage initiation criterion across the bonding region of each repair, the predicted location of failure initiation was determined prior to the complete failure of the cohesive zone. Figure 12 shows the cohesive damage across half of the parent structures of a conventional 2° scarf and a fibre-oriented design with a minimum 2° taper. In the conventional 2° scarf repair, damage starts between the inner-most 0° plies; while in the fibre-oriented scarf repair, damage begins in a number of the stepped corners adjacent to the 0° plies. With the exception of the conventional 2° scarf that only sees damage initiation from the inner 0° ply, the sites for damage initiation remain consistent for the full range of taper angles (2°, 3°, 5° and 8°) of each repair configuration, as depicted in Figure 13. Secondary and tertiary initiation sites are also seen in the conventional and fibre-oriented step repairs, which show more complex paths to failure than their scarfed counterparts.

7 Discussion

The simulation results suggest that the fibre-oriented step approach will not produce any significant benefit over a conventional step design. However, the fibre-oriented scarf design shows a considerable improvement in terms of strength, or size reduction, compared with the conventional scarf approach. It is expected that the stress concentrations at step corners and mergers are facilitating earlier damage initiation in the fibre-oriented step repairs compared with the other approaches. Alternatively, the fibre-

oriented scarf approach only introduces stepped sections in regions of reduced stress, which are not making as great a contribution to early damage initiation as in the fibre-oriented step configuration. This is demonstrated by only a small difference between the results of the simplified fibre-oriented scarf joint and the 3D repair case. For this work, it is important to note that the simulations rely on a brittle adhesive material, Araldite® AV138, and have been conducted under uniaxial load conditions. More ductile adhesives, or bi-axial load conditions, may not exhibit the same benefits from the fibre-oriented scarf approach.

Existing work by Niedernhuber et al. [14] reported a significant benefit in joint length reduction by employing a fibre-oriented step design as opposed to a conventional step approach. However, these tensile test results were achieved for step and fibre-oriented step joints with a minimum taper angle of 1.22° . This results in an equivalent taper of 2.12° for the fibre-oriented step joints. Given the trend of step joint results in Figure 9, it would not be surprising to see a marginal difference in conventional step joints with such shallow tapers. Hence, the benefit, if any, of a fibre-oriented step design cannot be properly assessed in this range. Fundamental testing with steeper taper angles will provide more reliable evidence to assess the performance of a fibre-oriented approach, for both step and scarf designs, since the expected change in strength between the joints will be more significant.

8 Conclusion

This work investigated the potential of optimised joint and repair geometries for adhesively bonded composite structures. The existing fibre-oriented step design has been considered and extended to a novel fibre-oriented scarf design that aims to improve the performance of bonded joints and repairs. A Matlab tool was developed to execute a parametric analysis of the effect of ply thickness, taper angle, number of plies and stacking sequence on the relative size reduction benefits of fibre-oriented designs. Significant benefits in terms of size reduction were indicated in composites with a greater ply thickness, greater number of plies or shallower taper. The stacking sequence, unless all plies are similarly aligned, appears to have little effect. Ultimately the minimum benefit, in terms of scarf area reduction, is 36% for a fibre-oriented approach compared with a conventional approach.

Cohesive Zone Models of conventional and fibre-oriented joints were developed, along with full 3D repair models, to compare the ultimate strength of the optimised designs. In both joints and repairs, the fibre-oriented step design appeared to show no significant benefit over conventional step repairs of a similar size. However the fibre-oriented scarf approach predicted 17-22% greater ultimate strength compared with similarly sized conventional scarf designs, or alternatively a size reduction of 33-40% for the same ultimate strength.

Acknowledgements

This research was conducted via Northern Ireland Advanced Engineering Competence Centre (NIAECC) funding in collaboration with Bombardier, CCP Gransden, Datum Tool Design and Wrightbus.

References

- [1] Baker AA. A Proposed Approach for Certification of Bonded Composite Repairs to Flight-Critical Airframe Structure. *Appl Compos Mater* 2011;18:337–69. doi:10.1007/s10443-010-9161-z.
- [2] Baker AA, Gunnion AJ, Wang J. On the Certification of Bonded Repairs to Primary Composite Aircraft Components. *J Adhes* 2015;91:4–38. doi:10.1080/00218464.2014.883315.
- [3] Whittingham B, Baker AA, Harman AB, Bitton D. Micrographic studies on adhesively bonded scarf repairs to thick composite aircraft structure. *Compos Part A Appl Sci Manuf* 2009;40:1419–32. doi:10.1016/j.compositesa.2008.12.011.
- [4] Wang CH, Gunnion AJ. On the design methodology of scarf repairs to composite laminates. *Compos Sci Technol* 2008;68:35–46. doi:10.1016/j.compscitech.2007.05.045.
- [5] Soutis C, Hu FZ. Strength Analysis of Adhesively Bonded Repairs. In: Tong L, Soutis C, editors. *Recent Adv. Struct. Joints Repairs Compos. Mater.*, Dordrecht: Springer Netherlands; 2003, p. 141–72. doi:10.1007/978-94-017-0329-1_5.
- [6] Caminero MA, Pavlopoulou S, Lopez-Pedrosa M, Nicolaisson BG, Pinna C, Soutis C. Analysis of adhesively bonded repairs in composites: Damage detection and prognosis. *Compos Struct* 2013;95:500–17. doi:10.1016/j.compstruct.2012.07.028.
- [7] Harman AB, Wang CH. Improved design methods for scarf repairs to highly strained composite aircraft structure. *Compos Struct* 2006;75:132–44. doi:10.1016/j.compstruct.2006.04.091.
- [8] Robson JE, Matthews FL, Kinloch AJ. The Strength of Composite Repair Patches: A Laminate

- Analysis Approach. *J Reinf Plast Compos* 1992;11:729–42. doi:10.1177/073168449201100702.
- [9] Breitzman TD, larve E V, Cook BM, Schoeppner GA, Lipton RP. Optimization of a composite scarf repair patch under tensile loading. *Compos Part A Appl Sci Manuf* 2009;40:1921–30. doi:10.1016/j.compositesa.2009.04.033.
- [10] Gunnion AJ, Herszberg I. Parametric study of scarf joints in composite structures. *Compos Struct* 2006;75:364–76. doi:10.1016/j.compstruct.2006.04.053.
- [11] Wang CH, Gunnion AJ. Optimum shapes of scarf repairs. *Compos Part A Appl Sci Manuf* 2009;40:1407–18. doi:10.1016/j.compositesa.2009.02.009.
- [12] Holtmannspötter J, Czarnecki J V, Feucht F, Wetzell M, Gudladt H-J, Hofmann T, et al. On the Fabrication and Automation of Reliable Bonded Composite Repairs. *J Adhes* 2015;91:39–70. doi:10.1080/00218464.2014.896211.
- [13] Bremer C. Efficient post-machining and automated repair. 20th Int. Conf. Compos. Mater., Copenhagen: 2015.
- [14] Niedernhuber M, Holtmannspötter J, Ehrlich I. Fiber-oriented repair geometries for composite materials. *Compos Part B Eng* 2016. doi:10.1016/j.compositesb.2016.03.027.
- [15] Campilho RDSG, de Moura MFSF, Domingues JMS. Modelling single and double-lap repairs on composite materials. *Compos Sci Technol* 2005;65:1948–58. doi:10.1016/j.compscitech.2005.04.007.
- [16] Campilho RDSG, Fernandes TAB. Comparative Evaluation of Single-lap Joints Bonded with Different Adhesives by Cohesive Zone Modelling. *Procedia Eng* 2015;114:102–9. doi:10.1016/j.proeng.2015.08.047.
- [17] Ridha M, Tan VBC, Tay TE. Traction-separation laws for progressive failure of bonded scarf repair of composite panel. *Compos Struct* 2011;93:1239–45. doi:10.1016/j.compstruct.2010.10.015.

List of Figures

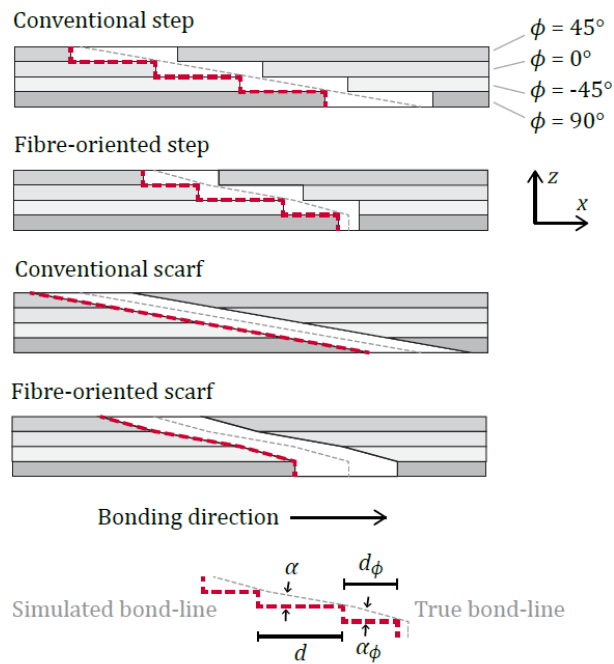


Figure 1: Different bonding configurations for a composite $[45^\circ, 0^\circ, -45^\circ, 90^\circ]$ layup.

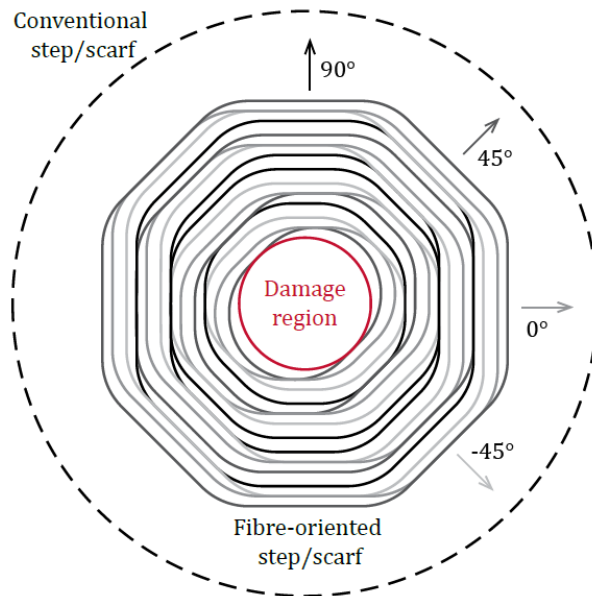


Figure 2: Ply profiles for a fibre-oriented step/scarf repair in a $[45^\circ, 0^\circ, -45^\circ, 90^\circ]_{2s}$ laminate compared with the size of a conventional step/scarf repair.

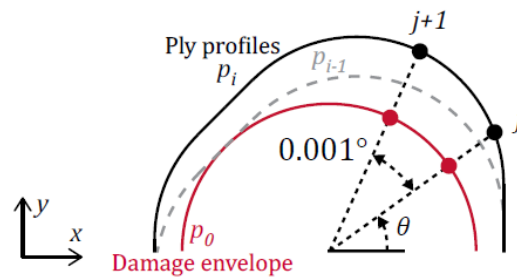


Figure 3: Definition of the j^{th} point on the i^{th} ply profile, with an 0.001° angular resolution between points.

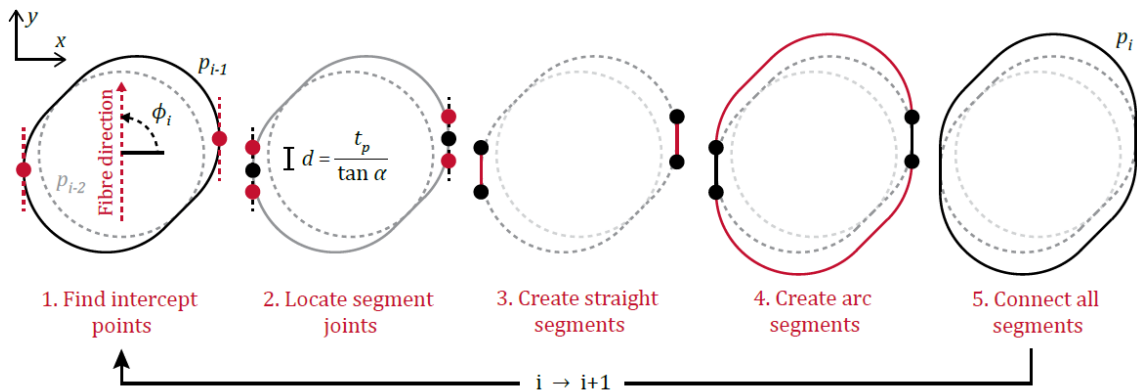


Figure 4: Process for the definition of fibre-oriented ply profile, p_i , based on ply orientation, ϕ_i , ply thickness, t_p , scarf angle, α , and the previous ply profile, p_{i-1} .

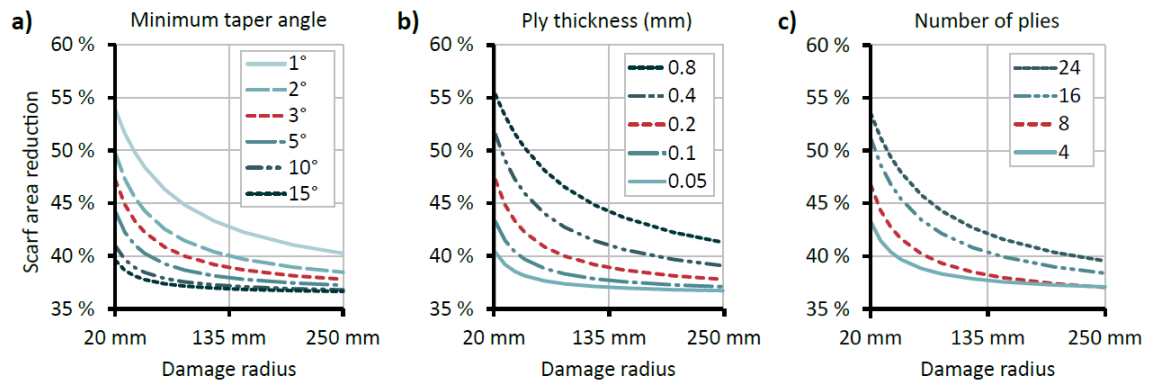


Figure 5: The effects of, a) minimum taper angle, b) ply thickness and, c) number of plies, on scarf area reduction for fibre-oriented methods, against damage radius. Dashed red curves represent the baseline results across each change in variable (3° minimum taper angle, 0.2 mm ply thickness and $8 \text{ ply } [45^\circ, 0^\circ, -45^\circ, 90^\circ]$ layup).

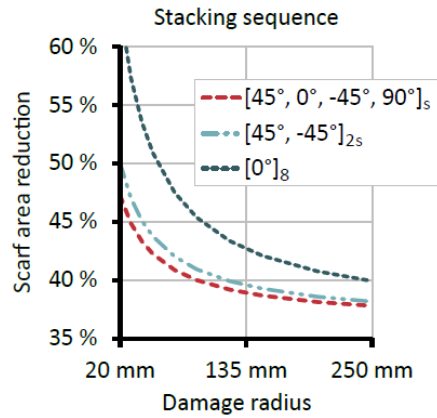


Figure 6: The effect of stacking sequence on scarf area reduction, against damage radius. All curves are for 3° minimum taper angle and 0.2 mm ply thickness.

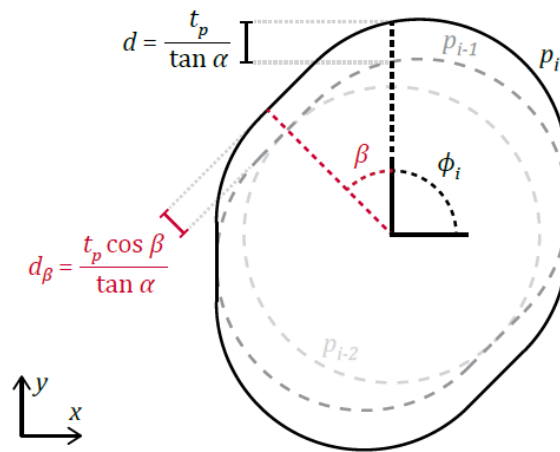


Figure 7: Change in bonding region length for a fibre-oriented repair in any direction, β , based on fibre orientation, ϕ_i , minimum taper angle, α , and ply thickness, t_p .

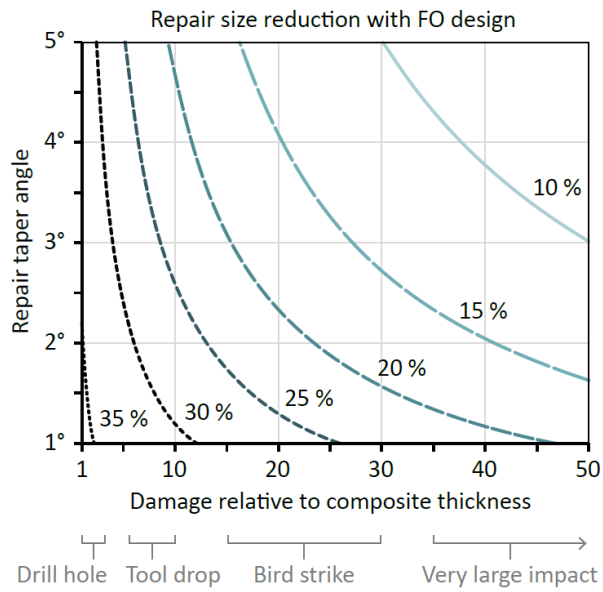


Figure 8: Reduction in overall repair size (compared to a standard scarf repair) resulting from a fibre-oriented approach for a range of taper angles and damage size.

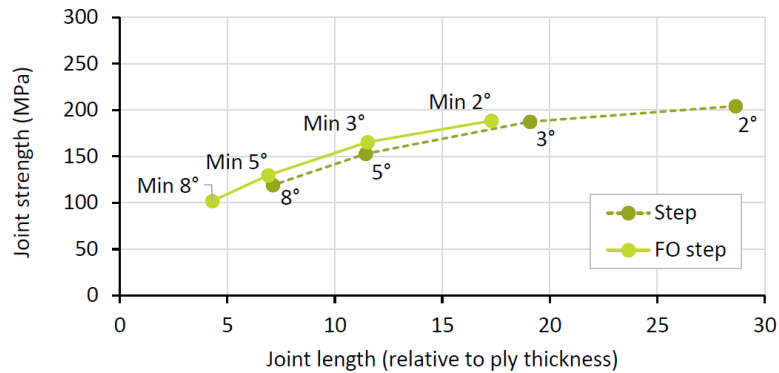


Figure 9: Simulated tensile strength of step and fibre-oriented step joints with various taper angles.

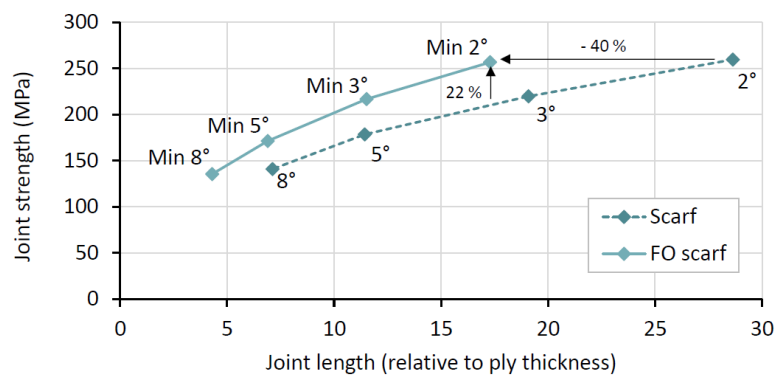


Figure 10: Simulated tensile strength of scarf and fibre-oriented scarf joints with various taper angles.

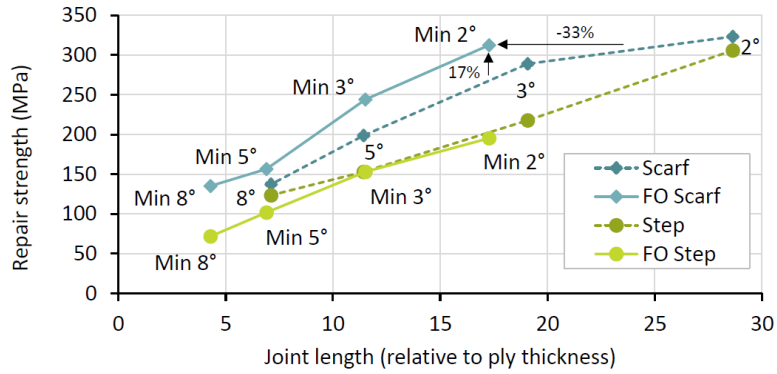


Figure 11: Simulated tensile strength of step, scarf, fibre-oriented step and fibre-oriented scarf repairs with various taper angles.

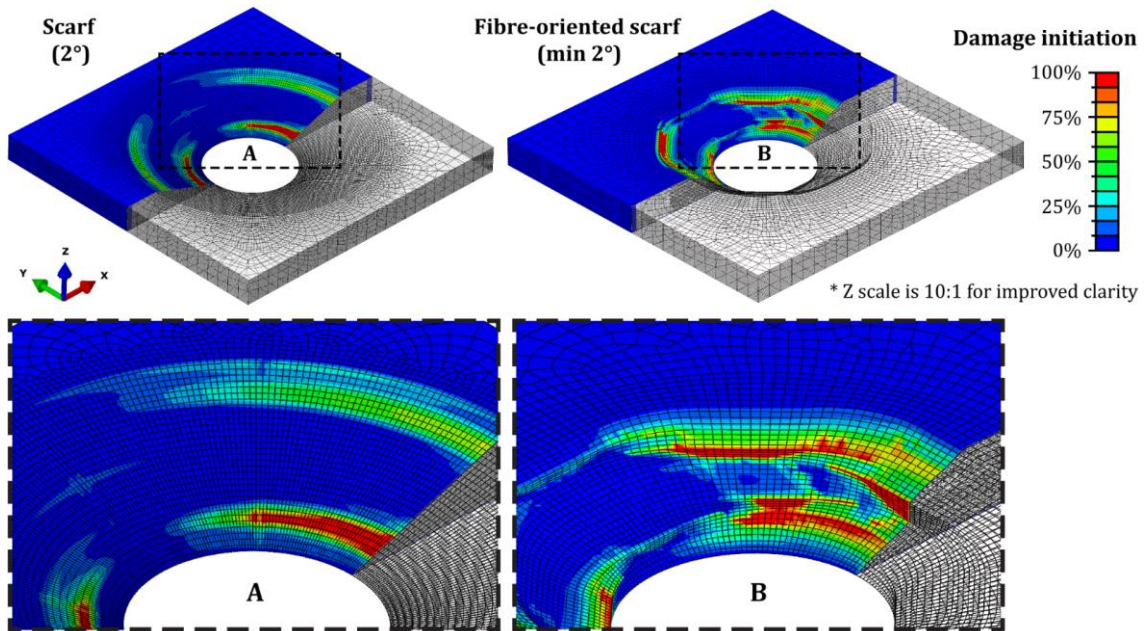


Figure 12: Simulated damage initiation in the 2° scarf and min 2° fibre-oriented scarf repairs, immediately prior to complete cohesive failure across the entire bonding region. Note, the Z scale has been artificially increased by a factor of 10, and the models displayed in half-wireframe, for better visualisation of the repair interfaces and cross-sections.

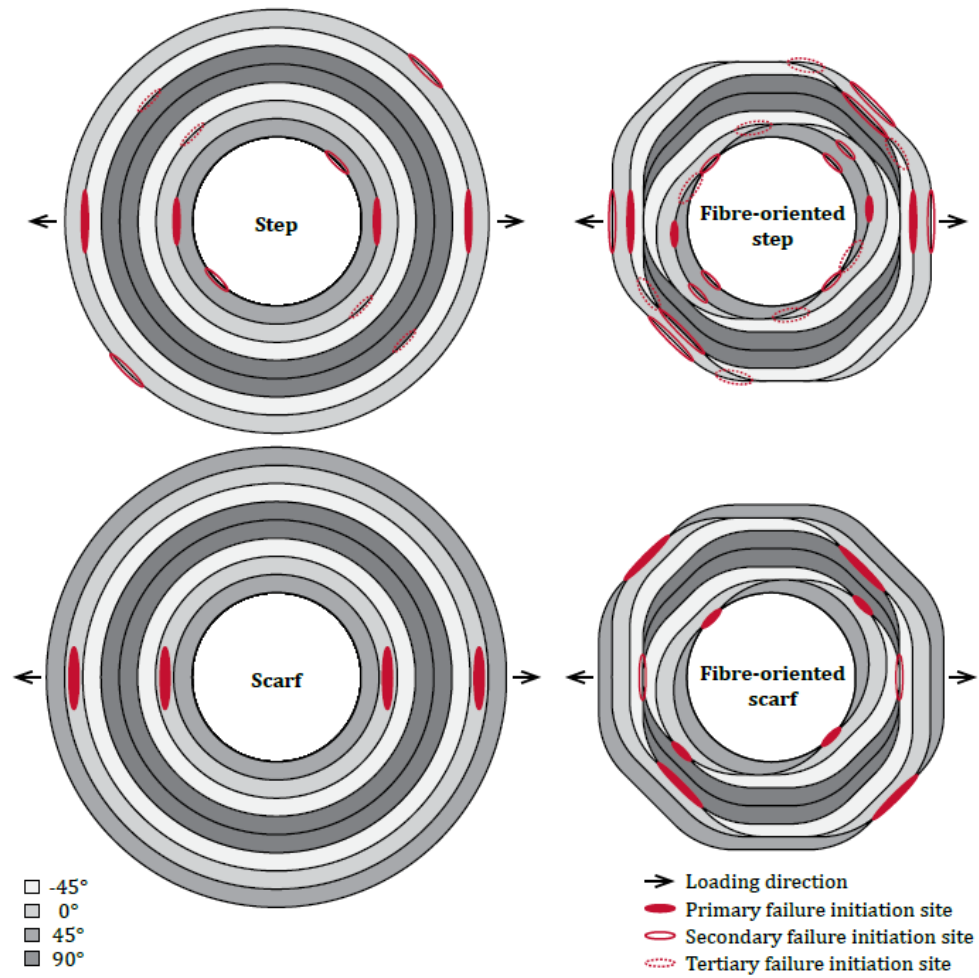


Figure 13: Common sites for damage initiation in the simulated adhesive bonding regions of conventional and fibre-oriented repairs.

List of Tables

Table 1: List of variables for parametric study (underlined variables represent the baseline parameters).

Parameter	Variable range
Initial damage envelope radius (mm)	20, 30, 40, 50, 70, 90, 120, 150, 200, 250
Minimum taper angle	1°, 2°, <u>3°</u> , 5°, 10°, 15°
Ply thickness (mm)	0.05, 0.1, <u>0.2</u> , 0.4, 0.8
Number of plies	4, <u>8</u> , 16, 24
Stacking sequence	[0°] _x , [45°, -45°] _x , [0°, 60°, -60°] _x , [<u>45°</u> , 0°, -45°, 90°] _x

Table 2: Mechanical materials properties for composite lamina [15].

Property	Symbol (units)	Value
Young's modulus	E_1 (MPa)	109000
	$E_2 = E_3$ (MPa)	8819
Poisson's ratio	$\mu_{12} = \mu_{13}$	0.342
	μ_{23}	0.38
Shear modulus	$G_{12} = G_{13}$ (MPa)	4315
	G_{23} (MPa)	3200
Density	ρ (kg/m ³)	1800

Table 3: Properties for Araldite® AV138 adhesive [16] and the Cohesive Zone Model.

Property	Symbol (units)	Value
Young's modulus	E (MPa)	4890
Shear modulus	G (MPa)	1560
Adhesive thickness	t_a (m)	0.0002
Uncoupled traction-separation behaviour	K_{nn} (N/m ³)	24.45×10^{12}
	$K_{ss} = K_{tt}$ (N/m ³)	7.8×10^{12}
Damage initiation	t_{n0} (MPa)	39.45
	t_{s0} (MPa)	30.2
Fracture energy for damage evolution	$J_{c,I}$ (N/m)	200
	$J_{c,II}$ (N/m)	380